



Sharif University of Technology

Scientia Iranica

Transactions F: Nanotechnology

www.scientiairanica.com



Synthesis of graphene/gold hybrid nanomaterials by poly(ethylene glycol) linkers

M. Adeli^{a,*}, F. Madani^a and P. Sasanpour^b

a. *Department of Chemistry, Faculty of Science, Lorestan University, Khoramabad, Iran.*

b. *Department of Medical Physics and Biomedical Engineering, Faculty of Medicine, Shahid Beheshti University of Medical Sciences, Tehran, Iran.*

Received 7 September 2013; received in revised form 12 April 2014; accepted 28 July 2014

KEYWORDS

Gold nanorod;
Photothermal effect;
Graphene oxide;
Cancer therapy;
Polyethylene glycol.

Abstract. Herein, we report a simple approach for increasing the photothermal conversion efficiency of Gold Rods (GRs) as a result of interaction between gold rod and graphene oxide. For preparation of these hybrid materials, gold rods were synthesized and modified using functionalized polyethylene glycol-triazine (PEG-T). Then functionalized gold rods (GR-P) were attached to Graphene Oxide (GO) sheets by π - π stacking. It was found that GR-P coating can improve the stability of GO in aqueous solutions. Moreover cellular experiments showed that GR-P coating on GO induce remarkably reduced cell toxicity. Gold rod-graphene oxide (GR-P-GO) hybrid materials hold great promise for application in various biomedical fields such as photothermal cancer therapy.

© 2014 Sharif University of Technology. All rights reserved.

1. Introduction

The gold nanorods (GNRs) and Graphene Oxide (GO) have attracted considerable attention because of their unique optical, chemical, and physical properties and prodigious potential applications in a various areas including biosensing [1-4], surface enhance Raman scattering [5,6], photoacoustic imaging [7-9], gene delivery [10-13], drug delivery [14-20], photothermal cancer therapy [21-24] etc. GNRs and GO have been used as heat sources for hyperthermia, due to their strongly enhanced absorption in NIR regions and producing heat via non-radiative electron relaxation dynamic. So GNRs and GO are good candidates for efficient photothermal ablation of tumors. Nevertheless, the clinical applications of GNRs have been limited, due to high cytotoxicity of CTAB that covers the surface of GNRs and is essential for their stabilization and also prevents the aggregation of GNRs [25]. Therefore, it is necessary to modify the surface of CTAB-

passivated GNRs with biocompatible capping ligands such as phosphatidylcholine (PC) [26], polyethylene glycol (PEG) [27,28] etc., for cell-related studies. Modified ligands should also provide stability for GNRs in the aqueous phase [29,30].

Studies have shown that GO, in comparison with single-walled nanotubes (SCNT) [31], is a more effective photothermal system, and, on the other hand, has a better biocompatibility with biological environment [32]. It also in a longer period of time, stays in circulation.

However, the toxicity of GO and its biocompatibility have not been fully understood still.

Several latest reports uncovered that as-prepared GO showed dose-dependent toxicity in vitro against cells [33]. After intravenous injection, GO would dominantly accumulated in lungs of mice over long periods of time, inducing obvious pulmonary toxicity [34,35]. Coating of biocompatible polymers on graphene may help to circumvent these problems.

Functionalization of graphene sheets with various chemical groups and inorganic nanoparticles, such as Ag, Au, TiO₂, and Fe₃O₄, can further enhance the

*. *Corresponding author. Tel: +98 9163603772
E-mail address: adeli@sharif.edu (M. Adeli)*

properties of graphene. Hybrid materials, consisting of nanoparticles distributed on the surface of graphene, could potentially display not only the unique properties of nanoparticles [36,37] and those of graphene [38-41], but also additional novel properties due to the interaction between the nanoparticles and the graphene.

As a result and based on the above explanation, incorporation of GNRs into GO lead to hybrid materials with unique properties.

The final goal of the current study is to investigate the photothermal effect of a GR assembly incorporated into a Graphene Oxide (GO) sheet, which is an ideal substrate material for meeting our objective because of its high thermal conductivity ($\sim 5,000 \text{ Wm}^{-1}\text{K}^{-1}$) and strong transmittance of light ($\sim 97.7\%$) [42,43]. In this work, hybrid materials, consisting of modified GR with Polymer (GR-P) and GO, were synthesized and characterized. In order to prepare GR-P-GO hybrid materials, GR-P was staked onto the surface of GO using a polyethylene glycol spacer. This system exhibits a useful absorbance of NIR light and consequently production of the heat.

2. Experimental section

Tetrachloroauric acid ($\text{HAuCl}_4 \cdot 3\text{H}_2\text{O}$) was purchased from Sigma, and sodium borohydride, silver nitrate, ascorbic acid, cetyltrimethyl ammonium bromide (CTAB), cysteamine (CY), cyanuric chloride, sodium hydride, methanol, dichloromethane and polyethylene glycol (PEG₁₀₀₀) were purchased from Merck.

Infrared (IR) experiments were performed using a Nicolet 320 FT-IR. Ultraviolet (UV) spectra were recorded on a Shimadzu (1650 PC) scanning spectrophotometer. Ultrasonic bath (Model: 5RS, 22 KHz, Made in Italy) was used to disperse materials in solvents. The particle size, polydispersity and zeta potential of materials were determined using Dynamic Light Scattering (DLS) (zetasizer ZS, Malvern Instruments). Surface imaging studies were performed using Atomic Force Microscopy (AFM) to estimate surface morphology and particle size distribution. Samples were imaged with the aid of Dualscope/Rasterscope C26, DME, Denmark, using DS 95-50-E scanner with vertical z-axis resolution of 0.1 nm.

2.1. Synthesis of GR

GR was synthesized using a NaBH_4 -ascorbic acid mixture [44]. In this typical synthesis, 10 mL of growth solution was prepared by dissolving HAuCl_4 (concentration 1 mM-100 mM) in aqueous CTAB solution. Next, AgNO_3 (concentration 0.1 mM-20 mM) and ascorbic acid solution (two equivalents with respect to gold salt) were mixed. The orange color of the gold salt disappears due to the reduction of Au^{3+} to Au^+ by ascorbic acid. Finally, 1-1000 mL of NaBH_4 (0.01 M)

solution was rapidly mixed and the color of the solution changed to deep brown/violet within a few minutes.

2.2. Preparation of polyethylene glycol triazine (PEG-T)

A solution of PEG and sodium hydroxide in water was added to a solution of cyanuric chloride in 50 mL of dichloromethane at 0°C . Then, the mixture was stirred at 0°C for 1 h and at room temperature for 1 h and was refluxed for an additional 6 h. The purified product was obtained as a white solid in a 100% yield [45-47].

2.3. Preparation of GR-P

The GRs were easily modified by alkanethiols. Chemical modification of GRs was achieved according to the following procedure: 150 μL of 25 mM aqueous solution of cysteamine was added to 5 mL of the GRs suspension and it was stirred for at least 20 min at room temperature. Then, GRs were collected by centrifugation at 8700 rpm for 12 min and resuspended in 5 ml distilled water. Then, 3 ml gold rods-cysteamine (GR-CY) solution, in ice bath, was added dropwisely to 1 ml of PEG-T (0.7 mM) solution. The mixture was stirred for 30 min. The resulting solution was under ultrasound for 1 h at 23°C and was left to stand for 30 min at room temperature. Then it was purified by centrifugation for 10 min at 8700 rpm and resuspended in 5 ml distilled water and stored at 4°C .

2.4. Preparation of GR-P-GO hybrid material

GO produced according to the Hummers method [48], especially synthesized from natural graphite can be easily dispersed in water. According to, a desired amount of GO powder (0.5 mg) was dispersed into 5 mL of distilled water and it was treated by mild ultrasound for 15 min in order to form a homogeneous suspension. 150 μL of GR-P was added to the suspension under stirring, and the mixture was sonicated for 30 min and was stored at room temperature for a night. Then it was purified by centrifugation for 15 min at 11000 rpm, and resuspended in 5 ml distilled water, and was stored at 4°C .

2.5. Preparation of GR-GO hybrid material

0.5 mg of GO powder was dispersed into 5 mL of distilled water and it was treated by mild ultrasound for 15 min in order to form a homogeneous suspension. 100 μL of GR was added to the suspension under stirring. The mixture was sonicated for 30 min and was stored at room temperature, then purified by centrifugation for 15 min at 11000 rpm and resuspended in 5ml distilled water and storage at 4°C .

2.6. Cell viability assay (MTT)

Colorimetric assay is a popular method in quantifying cell survival percentage. In principle, the absorbance of formazan which was produced from the mitochondrial oxidation of 3-(4, 5-dimethylthiazolyl-

2)-2,5-diphenyltetrazolium bromide (MTT) in living cells is directly proportional to the number of living cells. Briefly, HeLa cells were seeded into 96-well plates with 200 μ L medium (DMEM) and incubated for 24 h at 37°C under a 5% CO₂ atmosphere. Then, 20 μ L GR, GR-P, GO, GR-GO and GR-P-GO were incubated for 24 h, 48 h and 72 h, respectively. After that, 0.05 mg of MTT was added to each well and the plates were incubated for 2 h. Next, the MTT solutions were removed and 100 μ L DMSO (Dimethylsulfoxide) was added to each well. Then the absorbances of the wells at 490 nm were measured with a microplate reader. The obtained cell viability was expressed as a percentage relative to cells incubated with medium only.

Cell viability was calculated using the equation:

$$\text{Cell viability (\%)} = (\text{Ints}/\text{Intscontrol}) \times 100,$$

where “Ints” is the colorimetric intensity of the cells incubated with the samples, and “Intscontrol” is the colorimetric intensity of the cells incubated with the Media only (positive control).

3. Results and discussion

In this work, GRs with CTAB capping agent were synthesized and then CY was used to replace CTAB molecules on the surface of GRs. Functionalized polyethylene glycol was then conjugated to the surface of the resultant cysteamine-modified GRs (GR-CY) (Scheme 1).

GRs were deposited onto the surface of GO using electrostatic interaction between the negative GO and positive GRs surfaces (Scheme 2(a)). For preparation of GR-P-GO hybrid materials, GR-P was staked onto the surface of GO by interactions between π systems of triazine and graphene oxide (Scheme 2(b) and (c)).

IR spectra were used to prove the synthesis of GR-P and GR-P-GO and evaluate interactions between their species. Figure 1 shows the IR spectrum of GR, CY, GR-CY, PEG-T and GR-P. As we discussed in the previous section, GR has been established in the medium by CTAB surfactant. In IR spectrum of GNR (Figure 1(a)) absorption bands at 2981, 2848.57 cm^{-1} and 1342 cm^{-1} are corresponded to the stretching vibration of C-H and C-N bands, respectively. Also CH₂ and CH₃ bending vibration appeared at 1481 and 1360 cm^{-1} , respectively. In absorption spectrum of CY, symmetric stretching bond of N-H, asymmetric stretching bond of N-H, N-H bending vibration, C-N stretching and S-H stretching are shown at 3288, 3352, 1585, 1022 and 2550 cm^{-1} , respectively (Figure 1(b)). The vibration bond of S-H group that is seen as a weak bond in systeamine spectrum disappeared at IR spectrum of GR-CY (Figure 1(c)), and this shows the

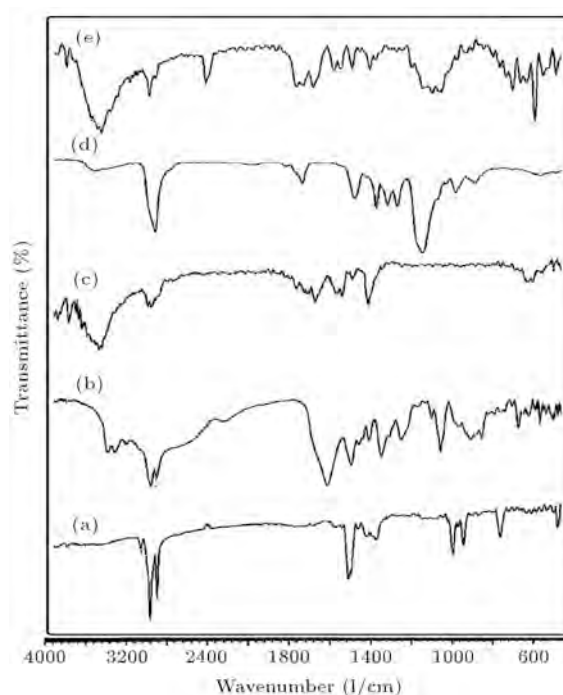
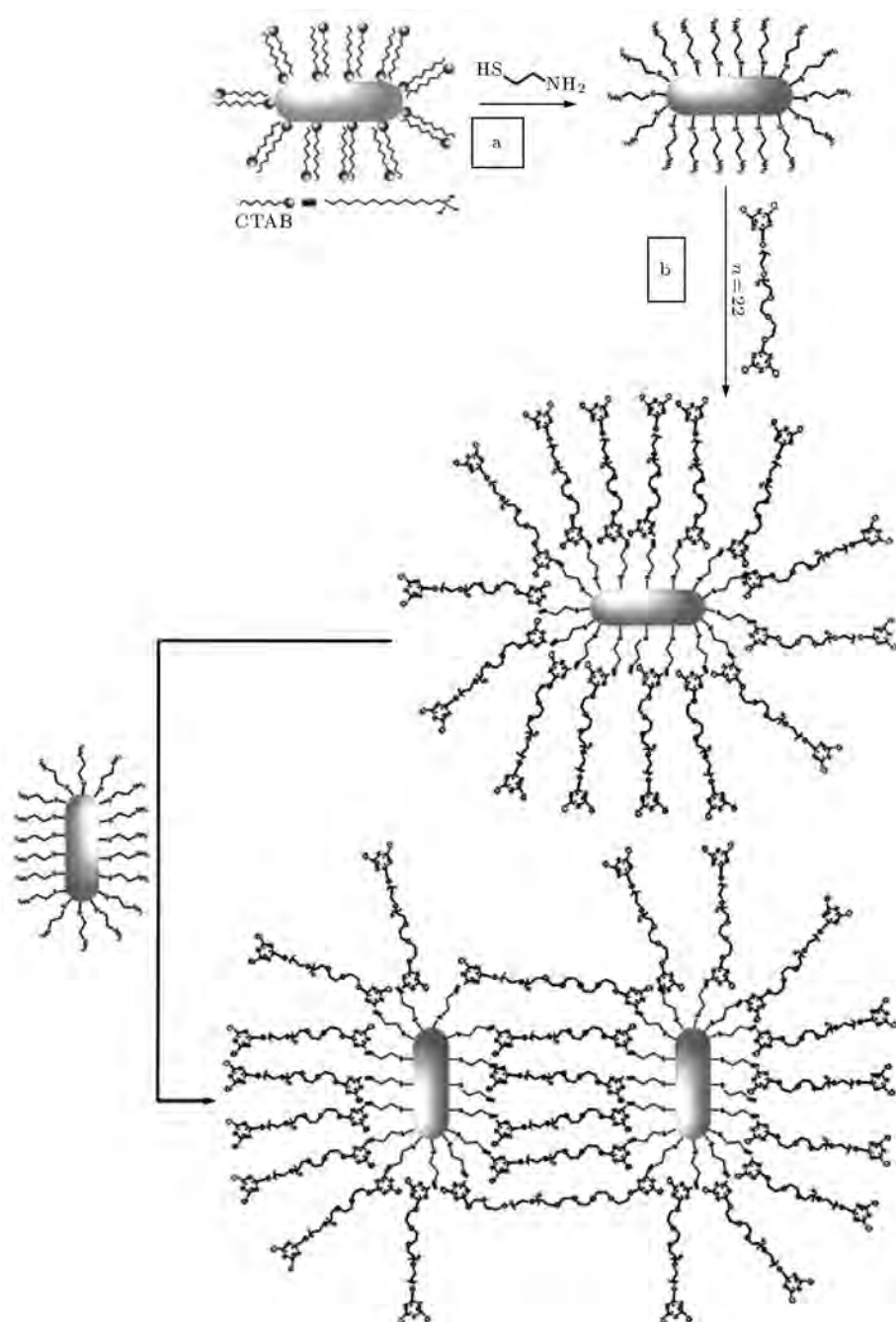


Figure 1. IR Spectra of a) GR, b) cysteamine, c) GR-CY, d) PEG-T, and e) GR-P.

formation of covalent bond between thiol group and GR surface. Figure 1(d) shows the IR spectrum of PEG-T. The absorption bond of C-O stretching at 1106 cm^{-1} and C=N of triazine ring at 1724 cm^{-1} are appeared. In IR spectrum of GR-P, the double peak of NH₂ of CY on the GR surface at 3398 cm^{-1} is changed to a single peak upon conjugation to the triazine group. Figure 2 shows the IR spectrum of GO, GR-GO and GR-P-GO. In IR spectrum of GO, six absorbance bands assigned to the stretching vibration of acidic OH, C=O, C-O (epoxy), C-O-C, C-OH, and C=C of aromatic ring can be seen at 3421, 1722, 1225, 1054, 1420 and 1627 cm^{-1} , respectively (Figure 2(a)). Presence of vibration bands at 2920 and 2856 cm^{-1} corresponded to the C-H group of surfactant CTAB on GR surface in the IR spectra of GR-GO prove stacking of the GR on the surface GO (Figure 2(b)). Comparison of the absorbance bands of different species of GR-P-GO with the IR spectrum of this compound and shifted absorption bands shows the interaction between modified GR and GO. In IR spectrum of this system, absorption bands of OH and C=O acidic groups of GO are shifted from 1728 and 3407 cm^{-1} to 1726 and 3417 cm^{-1} , respectively. It shows that one of interactions between GR-P and GO is hydrogen bonding between acidic OH of GO and nitrogen atom in triazine ring. On the other hand, vibration of C=C of GO shifted from 1627 cm^{-1} to 1620 cm^{-1} in GR-P-GO hybrid material proving interactions between terminated triazine in PEG and aromatic rings of GO (Figure 2(c)).

In UV-vis spectra, in general, GNRs have two



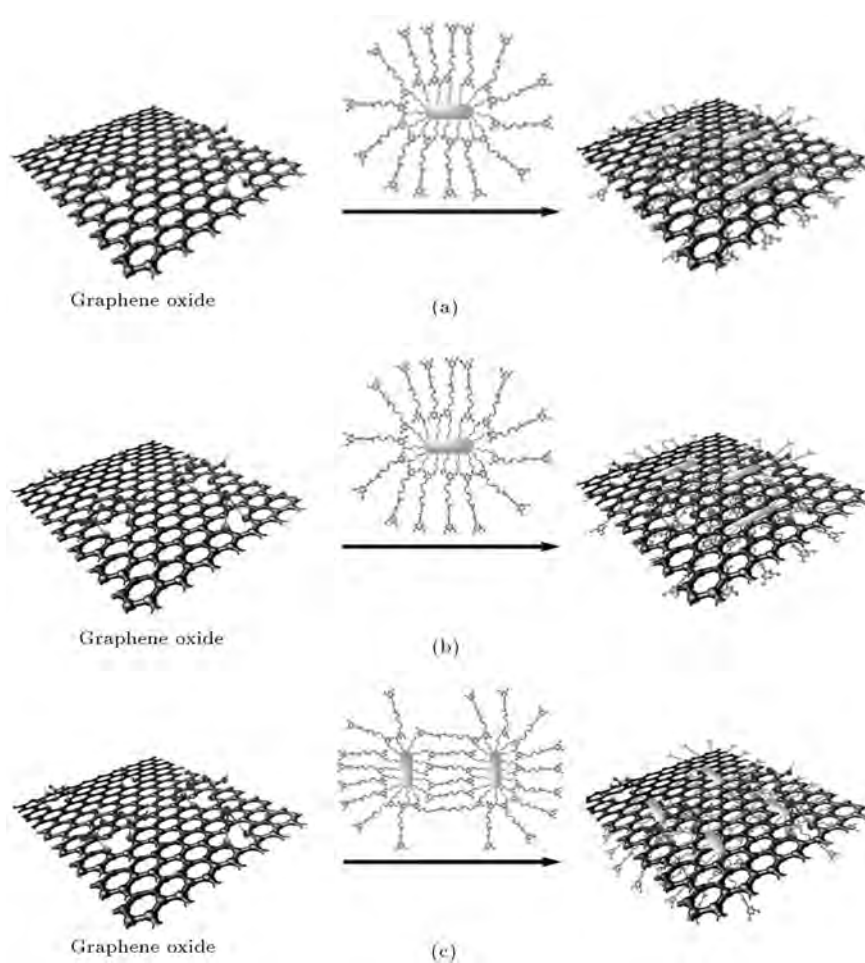
Scheme 1. Synthetic route for preparation of modified gold rod: a) Water, 25°C, 1h; and b) water, 0-25°C, 1 : 30'.

distinctive adsorption bands, namely, the transverse band and the longitudinal band, corresponding to the oscillation of free electrons along the short and long axis of GNR, respectively. In GR aqueous solution, the GRs have two absorption maxima, one at 520 nm, is attributed to the transverse surface plasmon resonance, and the other one at 720 nm corresponds to the longitudinal surface plasmon (SPL) resonance (Figure 3(a)). The modification of GRs by CY and functionalized poly ethylene glycol was monitored by UV-Vis absorption spectra as shown in Figure 3(b) and (c). The longitudinal and transverse plasmon

bands shifted from 720 nm to 870 nm and 520 nm to 530 nm, respectively, upon binding of cysteamine onto the surface of GRs (GR-CY), because of increasing the aspect ratio and size of GRs. After modification by polymer, a red-shift can be observed in the transverse band from 530 (Figure 3)) to 546 nm, because of the end-to-end assembly of GRs.

Also Figure 3 shows that aqueous solutions of GR, GR-CY and GR-P are completely stable at room temperature over several months and there is no observed aggregation.

The UV-vis spectra of GO was recorded (Fig-



Scheme 2. Synthetic route for preparation of GR-GO and GR-P-GO hybrid nanomaterials: a), b), and c) water, 25°C, 2 : 30'.

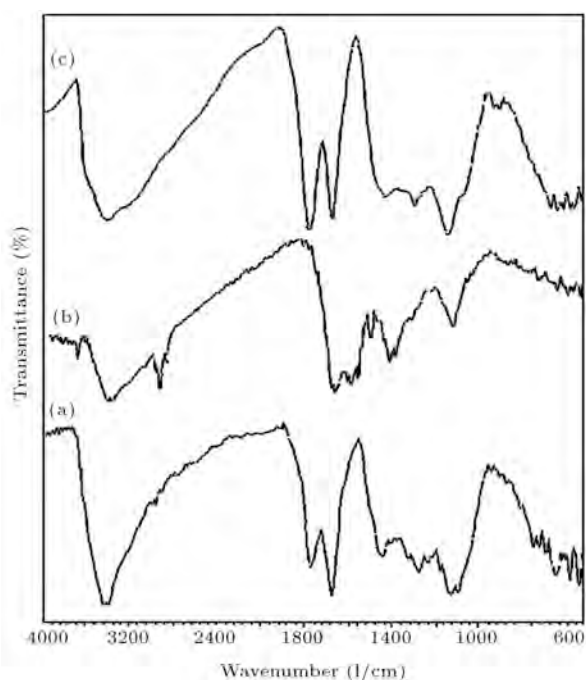


Figure 2. IR Spectra of a) GO, b) GR-GO, and c) GR-P-GO.

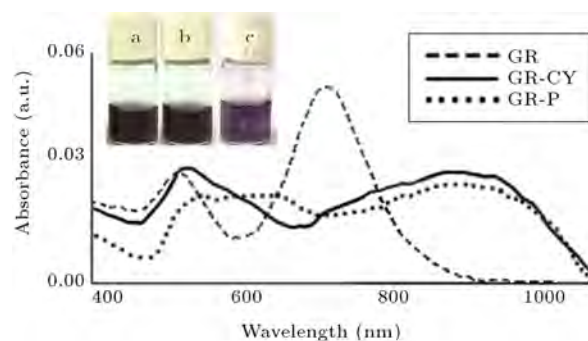


Figure 3. UV-vis spectra of a) GR, b) GR-CY, and c) GR-P and aqueous solutions of a) GR, b) GR-CY, and c) GR-P in 25°C.

ure 4(a)) showing a similar absorption peak at 230–240 nm, which was originated from the π -plasmon of carbon [49,50]. Successful GR and GR-P loading on GO were evidenced by UV-vis spectra of GR-GO and GR-P-GO hybrid nanomaterials (Figure 4) in which the characteristics of GR and GR-P absorption peaks were clearly identified (Figure 3(b) and (c)). The UV-vis peaks at 520 nm and 720 nm, and also 546 nm and 870 nm were then used to determine the concen-

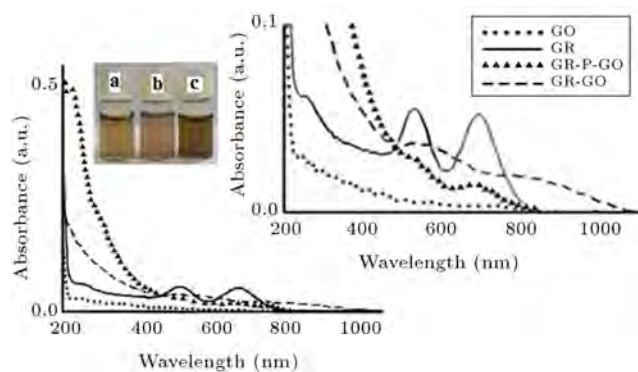


Figure 4. UV-vis spectra and UV-vis expanded spectra of GO, GR, GR-P-GO, and GR-GO and aqueous solutions of a) GO, b) GR-GO, and c) GR-P-GO at 25°C.

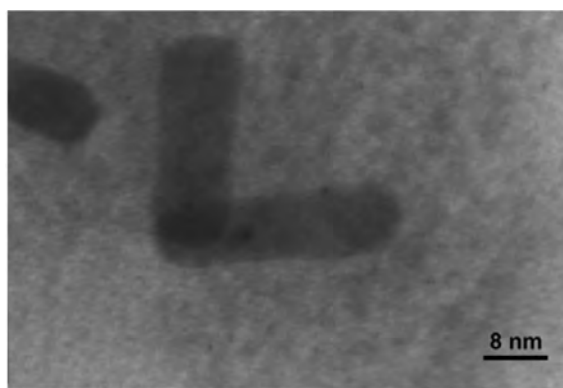


Figure 5. TEM image of GR.

trations of GR and GR-P in GR-GO and GR-P-GO samples after subtraction of absorbance contributed by GO. These changes can be seen in UV-vis expanded spectra clearly (Figure 4). In addition, Figure 4 shows that aqueous solutions of GO, GR-GO and GR-P-GO hybrid nanomaterials were stable at ambient conditions over several months, and no precipitation was observed.

TEM images were prepared by deposition of a suitable amount of the concentrated GRs (centrifuged and resuspended in distilled water) onto the carbon-coated copper grid. Figure 5 shows TEM image of synthesized GRs. The average dimension of GRs was estimated to be 360 nm long and 130 nm wide which represents an aspect ratio of 2.77. This feature can be also characterized by the longitudinal peak in the absorption spectrum.

Figure 6 shows a TEM image of GO sheets. The suspended graphene membranes presented here consist of single layer or bilayer sheets with average dimensions of 2 μm .

The morphology of GO before and after loading GR-P was characterized with AFM, as shown in Figure 7(a). GO shows a height of 1.3 nm, suggesting a single layer graphene sheet [51]. Figure 7(b) shows AFM images of GR-P-GO hybrid materials. A smooth surface can be seen for pristine GO (Figure 7(a)), while

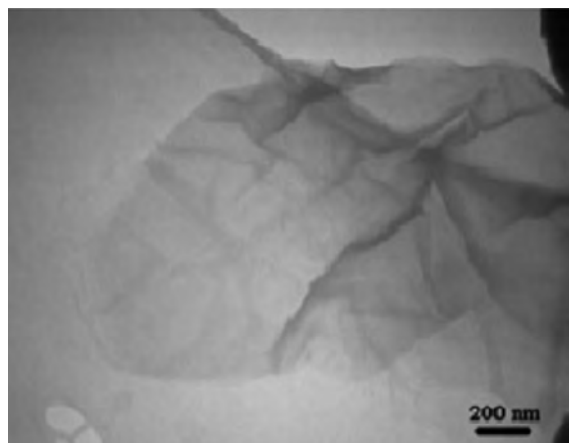


Figure 6. TEM image of GO.

Table 1. Zeta potential values of samples.

Sample	Zeta potential (mV)
GR	+33.18
GR-P	+8.29
GO	-20.51
GR-GO	-10.23
GR-P-GO	-31.98

many protuberances are observed for GR-P-GO hybrid (Figure 7(b)). These protuberances can be seen clearly in Figure 7(c) and (d). As can be observed, GRs-P uniformly are placed on the surface of GO. AFM phase contrast image of the GR-P-GO hybrid materials confirms this result. Phase contrast images show a network-like shape with two phases for GR-P-GO hybrid material. Dark parts are assigned to the GRs-P on the surface of GO and bright points correspond to GO. It was also observed that the average thickness of GR-P-GO sheets was 3.46 nm, while single layer GO sheets were 1.3 nm. The increased sheet thickness was attributed to the GR-P coating on graphene.

The zeta potential of synthesized hybrid materials was investigated in water and at 25°C by Dynamic Light Scattering (DLS). Useful information about interaction between GR, Polymer, and GO were obtained using zeta potential. Table 1 shows the zeta potential of GR which is 33 mV due to the presence of cationic surfactant CTAB. Replacing this surfactant by polymer changes GR's zeta potential to 8.26 mV. The positive zeta potential of polymer is due to the protonation of nitrogen atoms of triazine rings. Due to the presence of carboxylic groups on the surface of GO its zeta potential is -20.51 mV. The zeta potential of GR-GO hybrid material is -10.23 mV, because charge of surfactant of GR and CTAB is positive, and it is negative for GO.

Emission spectra of the GR, GR-P, GO and GR-P-GO under excitation by a 480 nm light are depicted

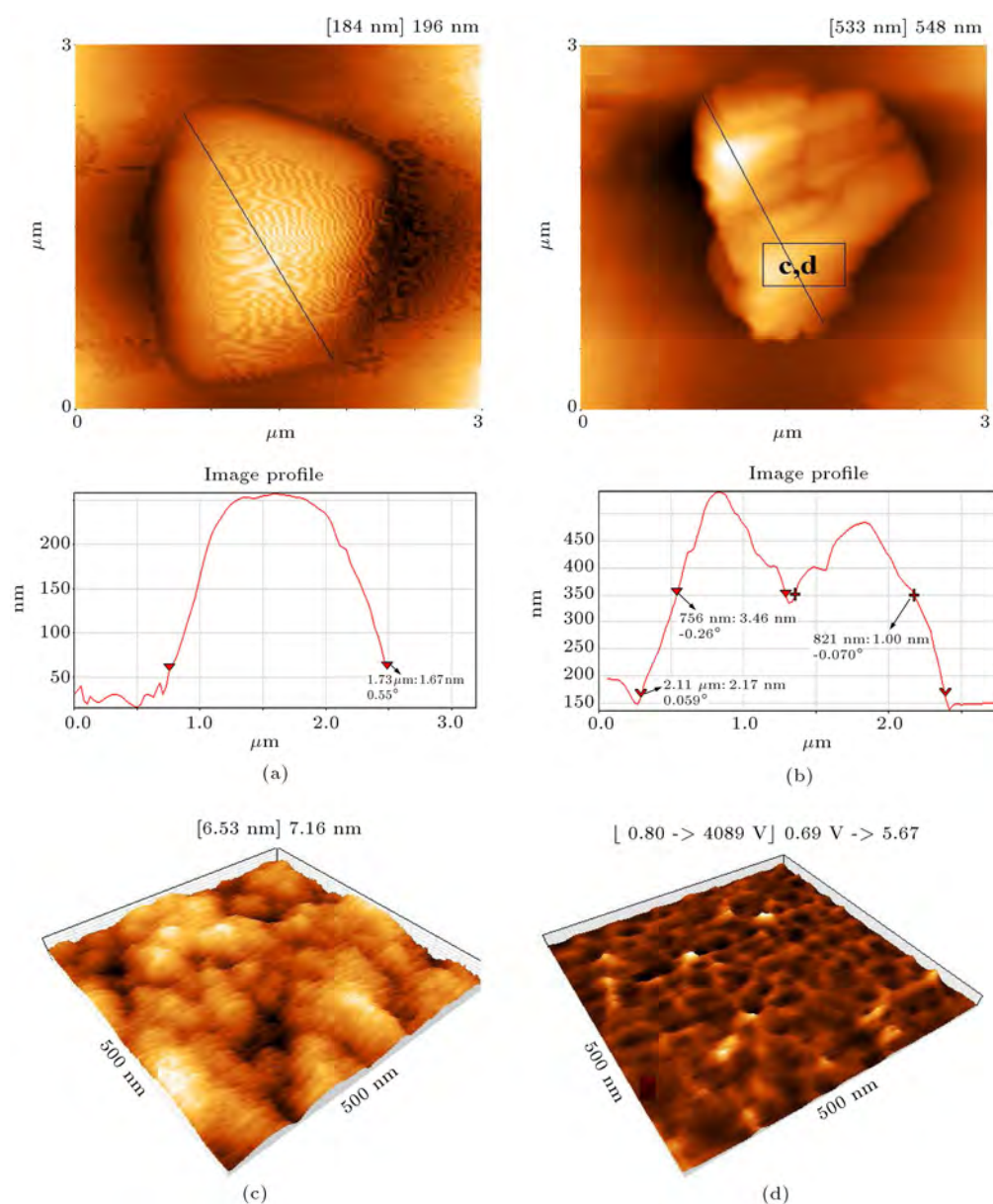


Figure 7. Topographic and profile AFM images of (a) GO and (b) GR-P-GO. Topographic (c), and the phase contrast (d) images of the region are shown inside the topographic AFM image of GR-P-GO.

in Figure 8. In this spectrum, free GR and GR-P exhibit a maximum luminescence emission at 523 nm and 578 nm, respectively. Because of the increasing aspect ratio of modified GRs, the emission spectrum is shifted to longer wavelengths, and its intensity decreases. However, GR-P-GO exhibits significant quenching at 578 nm emission band at the same excitation wavelength. These results indicate that there is a strong π - π stacking interaction between triazine of PEG-T in GR-P and aromatic rings of GO in GR-P-GO hybrid materials.

The ability of GRs and their modified forms to increase temperature of medium has also been investigated. Table 2 corresponds to the temperature of aqueous solutions of materials irradiated by 650

nm laser source with a power of 100 mW. It should be mentioned that the intensity of the present NIR laser is 10 times lower than the laser intensity ($> 2 \text{ W/cm}^2$) commonly used in previous reports. A low power source and the lower wavelength that materials respond were selected, because these two factors dominate the efficiency and safety of photothermal systems. Solutions of GR, GR-P, GO, GR-GO and GR-P-GO (800 μL) were irradiated in the plastic tubes. As can be seen, GR-P-GO hybrid materials increase temperature of solutions more than their precursors. There is a deficiency of information on the enhanced photothermal effect of GR, and to the best of our knowledge, this report is the first to demonstrate the increase in the photothermal efficiency derived from the

Table 2. Measured temperature of aqueous solutions of the sample after irradiation by a laser source at wavelength of 650 nm with a power 100 mW.

Sample	T_1-T_2 (°C)	Time (min)	Wavelength (nm)
GR	25.2-28.4	3	650
GR-P	25.2-31.7	3	650
GO	25.2-27.3	3	650
GR-GO	25.2-33.6	3	650
GR-P-GO	25.2-39.1	3	650

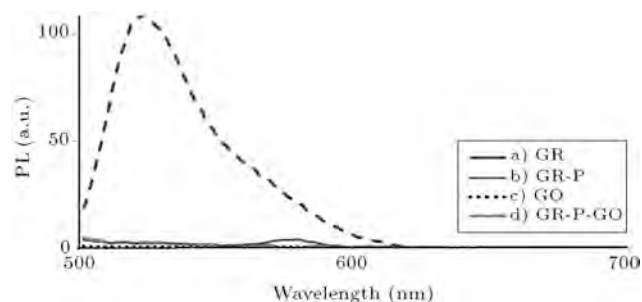


Figure 8. Luminescence spectra of a) GR, b) GR-P, c) GO, and d) GR-P-GO.

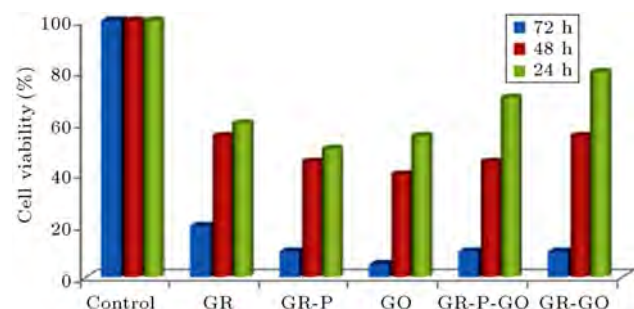


Figure 9. Cellular viability of HeLa cells, assessed by an MTT assay, after exposure to GR, GR-CY, GR-P, GO, GR-GO and GR-P-GO for 24, 48 and 72 h.

addition of GR-P onto the surface of GO. Therefore, the synthesized hybrid material can be used as new photothermal therapy systems with a high treatment efficacy.

All materials show a time-dependence toxicity (Figure 9). Interestingly, toxicity of materials increases abruptly in the first two days incubation, showing that this materials uptake by cells quickly. A reason for this observation could be the big size of materials. In this figure, because of higher dispersion and stability of GR-P in comparison with GR, the cellular uptake of GR-P is higher. Therefore, it reveals higher level of toxicity than GR. Also, due to the GO hydrophobic surface, GO exhibits higher cellular uptake and toxicity than GR-GO and GR-P-GO. On the other hand, GR-GO is bigger than GR-P-GO, hence the cellular uptake is low and toxicity is less.

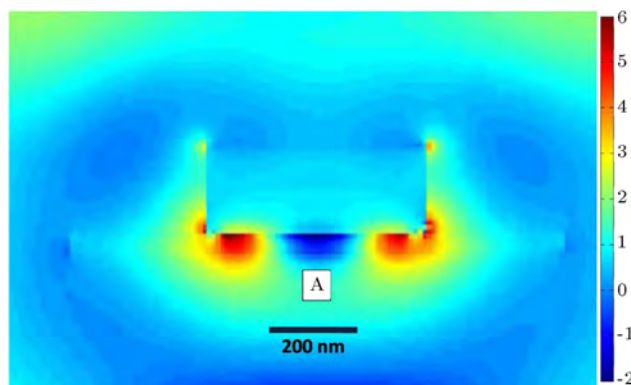


Figure 10. Electric field distribution around gold rod on graphene oxide substrate.

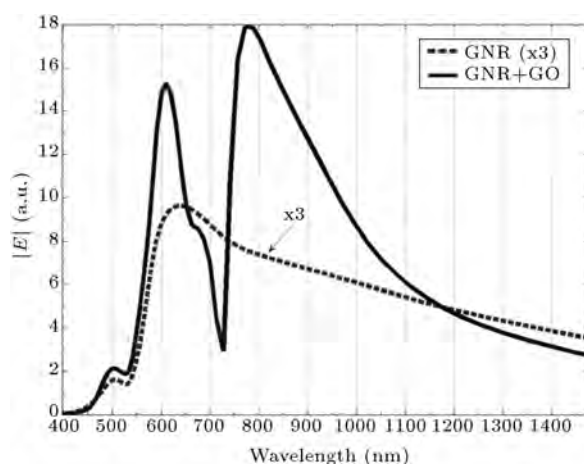


Figure 11. Electric field distribution spectrum at point A for two cases of Gold Rod (GR) and GR in vicinity of graphene oxide.

In order to model interaction of light with GR and GO, Maxwell's equations have been solved numerically. The chosen method is Finite-Difference Time-Domain technique [52]. In this method, in order to consider dispersion behavior of permittivity of GR, we have used the Drude-Lorentz model. In order to obtain the coefficients of the model, the relation should be fitted with parameters obtained by measurement [53], given by:

$$\varepsilon(\omega) = \varepsilon_{\infty} - \frac{\omega_D^2}{\omega^2 + i\gamma_D\omega} + \sum_{p=1}^2 \frac{\Delta\varepsilon_p\omega_p^2}{\omega_p^2 + 2i\omega\delta_p - \omega^2}. \quad (1)$$

Figure 10 shows electric field distribution around GR in vicinity of GO layer. Figure 11 presents calculated electric field spectrum (at point A of Figure 10), for two cases, simple GR and GR in vicinity of GO substrate. It can be seen from the spectrum of electric field that, in the presence of GO as substrate, enhancement of electric field is more. Also presence of peak around 760 nm will result in absorption of light in near IR region.

4. Conclusion

In summary, we offer a simple approach for increasing the photothermal conversion efficiency of GRs by interactions between gold rod and graphene oxide. Due to the efficient absorption of NIR light and consequently production of heat, the synthesized hybrid material can be used as a new and promising system for biomedical applications such as photothermal therapy.

References

- Wang, X., Li, Y., Wang, H., Fu, Q., Peng, J., Wang, Y., Du, J., Zhou, Y. and Zhan, L. "Gold nanorod-based localized surface plasmon resonance biosensor for sensitive detection of hepatitis B virus in buffer, blood serum and plasma", *Biosens. Bioelectron.*, **26**(2), pp. 404-410 (2010).
- Parab, H.J., Jung, Ch., Lee, J.H. and Park, H.G. "A gold nanorod-based optical DNA biosensor for the diagnosis of pathogens", *Biosens. Bioelectron.*, **26**(2), pp. 667-673 (2010).
- Akhavan, O., Ghaderi, Gh. and Rahighi, R. "Toward single-DNA electrochemical biosensing by graphene nanowalls", *ACS Nano.*, **6**(4), pp. 2904-2916 (2012).
- Eden, M.N. and Arben, M. "Graphene oxide as an optical biosensing platform", *Advanced Materials*, **24**(25), pp. 3298-3308 (2012).
- Huang, X., El-Sayed, I.H., Qian, W. and El-Sayed, M.A. "Cancer cells assemble and align gold nanorods conjugated to antibodies to produce highly enhanced, sharp, and polarized surface Raman spectra: A potential cancer diagnostic marker", *Nano Lett.*, **7**(6), pp. 1591-1597 (2007).
- Huanping, Y., Hailong, H., Zhenhua, N., Chee, K.P., Chunxiao, C., Jianyi, L. and Ting, Y. "Comparison of surface-enhanced Raman scattering on graphene oxide, reduced graphene oxide and graphene surfaces", *Carbon*, **62**, pp. 422-429 (2013).
- Qian, J., Jiang, Li., Cai, F., Wang, D. and He, S. "Fluorescence-surface enhanced raman scattering co-functionalized gold nanorods as near-infrared probes for purely optical in vivo imaging", *Biomaterials*, **32**(6), pp. 1601-1610 (2011).
- Chen, G. and Da-xiang, Cui. "Functionalized gold nanorods for tumor imaging and targeted therapy", *Cancer Biol Med.*, **9**(4), pp. 221-233 (2012).
- Manas, R., Tejas, S.K., Sandeep, K.M., Sunil, K.M., Sushil, K.S., Niroj, S., Kalpana, B., Raj, K.Sh., Debabrata, G. and Sabyasachi, S. "Graphene oxide from silk cocoon: A novel magnetic fluorophore for multi-photon imaging", *3 Biotech.*, **4**(1), pp. 67-75 (2014).
- Jain, P.K., Lee, K.S., El-Sayed, I.H. and El-Sayed, M.A. "Calculated absorption and scattering properties of gold nanoparticles of different size, shape, and composition: Applications in biological imaging and biomedicine", *J. Phys. Chem.*, **110**(14), pp. 7238-7248 (2006).
- Chen, Ch., Lin, Y.P., Wang, C.W., Tzeng, H.C., Wu, C.H., Chen, Y.C., Chen, C.P., Chen, L.C. and Wu, Y.C. "DNA-gold nanorod conjugates for remote control of localized gene expression by near infrared irradiation", *J. Am. Chem. Soc.*, **128**(11), pp. 3709-3715 (2006).
- Yamashita, S., Fukushima, H., Akiyama, Y., Niidome, Y., Mori, T., Katayama, Y. and Niidome, T. "Controlled-release system of single-stranded DNA triggered by the photothermal effect of gold nanorods and its in vivo application", *Bioorg. Med. Chem.*, **19**(7), pp. 2130-2135 (2011).
- Kim, H. and Kim, W.J. "Photothermally controlled gene delivery by reduced graphene oxide-polyethylenimine nanocomposite", *Small*, **10**(1), pp. 117-126 (2014).
- Pissuwan, D., Niidome, T. and Cortie, M. "The forthcoming applications of gold nanoparticles in drug and gene delivery systems", *J. Control. Release*, **149**(1), pp. 65-71 (2011).
- Niidome, T., Ohga, A., Akiyama, Y., Watanabe, K., Niidome, Y., Mori, T. and Katayama, Y. "Controlled release of PEG chain from gold nanorods: Targeted delivery to tumor", *Bioorg. Med. Chem.*, **18**(12), pp. 4453-4458 (2010).
- Sunil, P., Ritu, Sh., Ashmi, M., Mukeshchand, T., Goldie, Oza. and Madhuri, Sh. "Gold nanorods mediated controlled release of doxorubicin: nano-needles for efficient drug delivery", *Materials in Medicine*, **24**(7), pp. 1671-1681 (2013).
- Ghosh, P., Han, G., De, M., Kim, C. and Rotello, V.M. "Gold nanoparticles in delivery applications", *Adv. Drug Delivery Rev.*, **60**(11), pp. 1307-1315 (2008).
- Li, Z., Huang, P., Zhang, X., Lin, J., Yang, S., Liu, B., Gao, F., Xi, P., Ren, Q. and Cui, D. "RGD-conjugated dendrimer-modified gold nanorods for in vivo tumor targeting and photothermal therapy", *Mol. Pharm.*, **7**(1), pp. 94-104 (2009).
- Wei, Q., Ji, J. and Shen, J. "Synthesis of near-infrared responsive gold nanorod/PNIPAAm core/shell nanohybrids via surface initiated ATRP for smart drug delivery macromol", *Rapid Commun.*, **29**(8), pp. 645-650 (2008).
- Cassandra, L.W., Jaclyn, M.L., Xiliang, L. and Xinyan, T.C. "Electrically controlled drug delivery from graphene oxide nanocomposite films", *ACS Nano*, **8**(2), pp. 1834-1843 (2014).
- Jo, W., Freedman, K., Yi, D.K., Bose, R.K.S., Lau, K.K., Solomon, S.D. and Kim, M. "Photon to thermal response of a single patterned gold nanorod cluster under near-infrared laser irradiation", *J. Biofabrica.*, **3**(1), p. 015002 (2011).
- Ming, C., Heran, W., Zhen, Zh., Nan, L., Xiaohong, F. and Shanshan, X. "Gold nanorod-embedded electrospun fibrous membrane as a photothermal therapy

- platform”, *ACS Appl. Mater. Interfaces*, **6**(3), pp. 1569-1575 (2014).
23. Megan, A.M., Moustafa, R.K.A., Lauren, A.A., Rachel, D.N. and Mostafa, A.E. “The most effective gold nanorod size for plasmonic photothermal therapy: theory and in vitro experiments”, *J. Phys. Chem. B*, **118**(5), pp. 1319-1326 (2014).
 24. Akhavan, O. and Ghaderi, Gh. “Graphene nanomesh promises extremely efficient In vivo photothermal therapy”, *Small*, **9**(21), pp. 3593-3601 (2013).
 25. Alkilany, A.M., Nagaria, P.K., Hexel, C.R., Shaw, T.J., Murphy, C.J. and Wyatt, M.D. “Cellular uptake and cytotoxicity of gold nanorods: molecular origin of cytotoxicity and surface effects”, *Small*, **5**(6), pp. 701-708 (2009).
 26. Takahashi, H., Niidome, Y., Niidome, T., Kaneko, K., Kawasaki, H. and Yamada, S. “Modification of gold nanorods using phosphatidylcholine to reduce cytotoxicity”, *Langmuir*, **22**(1), pp. 2-5 (2006).
 27. Liao, H. and Hafner, L.H. “Gold nanorod bioconjugates”, *Chem Mater.*, **17**(18), pp. 4636-4641 (2005).
 28. Niidome, T., Yamagata, M., Okamoto, Y., Akiyama, Y., Takahashi, H., Kawano, T., Katayama, Y. and Niidome, Y. “PEG-modified gold nanorods with a stealth character for in vivo applications”, *J. Control. Release*, **114**(3), pp. 343-347 (2006).
 29. Lee, J., Yang, J., Seo, S.B., Ko, H.J., Suh, J.S., Huh, Y.M. and Haam, S. “Smart nanoprobe for ultrasensitive detection of breast cancer via magnetic resonance imaging”, *Nanotechnology*, **19**(48), pp. 485101-485111 (2008).
 30. Tavakoli, A., Adeli, M. and Vossoughi, M. “Synthesis of gold nanoparticle necklaces using linear-dendritic copolymers”, *European Polymer Journal*, **46**(2), pp. 165-170 (2010).
 31. Markovic, Z.M., Harhaji-Trajkovic, L.M., Todorovic-Markovic, B.M., Kepic, D.P., Arsin, K.M. and Jovanovic, S.P. “In vitro comparison of the photothermal anticancer activity of graphene nanoparticles and carbon nanotubes”, *Biomaterials*, **32**(4), pp. 1121-1129 (2011).
 32. Zhang, Y., Ali, S.F., Dervishi, E., Xu, Y., Li, Z. and Casciano, D. “Cytotoxicity effects of graphene and single-wall carbon nanotubes in neural pheochromocytoma-derived PC12 cells”, *ACS Nano*, **4**(6), pp. 3181-3186 (2010).
 33. Agarwal, S., Zhou, X., Ye, F., He, Q., Chen, G.C., Soc, J., Boey, F., Zhang, H. and Chen, P. “Interfacing live cells with nanocarbon substrates”, *Langmuir*, **26**(4), pp. 2244-2247 (2010).
 34. Wang, K., Ruan, J., Song, H., Zhang, J., Wo, Y., Guo, S. et al. “Biocompatibility of graphene oxide”, *Nanoscale Res Lett.*, **6**(1), pp. 1-8 (2010).
 35. Zhang, X.Y., Yin, J.L., Peng, C., Hu, W.Q., Zhu, Z.Y., Li, W.X. et al. “Distribution and biocompatibility studies of graphene oxide in mice after intravenous administration”, *Carbon*, **49**(3), pp. 986-995 (2010).
 36. Alivisatos, A.P. “Semiconductor clusters, nanocrystals, and quantum dots”, *Science*, **271**(5251), pp. 933-937 (1996).
 37. Fissan, H., Kennedy, M.K., Krinke, T.J. and Kruis, F.E. “Nanoparticles from the gas phase as building blocks for electrical devices”, *J. Nanopart. Res.*, **5**(3-4), pp. 299-310 (2003).
 38. Geim, A.K. and Novoselov, K.S. “The rise of graphene”, *Nat. Mater.*, **6**(3), pp. 183-191 (2007).
 39. Novoselov, K.S., Geim, A.K., Morozov, S.V., Jiang, D., Zhang, Y., Dubonos, S.V., Grigorieva, I.V. and Firsov, A.A. “Electric field effect in atomically thin carbon films”, *Science*, **306**(5696), pp. 666-669 (2004).
 40. Novoselov, K.S., Jiang, D., Schedin, F., Booth, T.J., Khotkevich, V.V., Morozov, S.V. and Geim, A.K. “Two-dimensional atomic crystals”, *P. Natl. Acad. Sci. USA*, **102**(30), pp. 10451-10453 (2005).
 41. Novoselov, K.S., Morozov, S.V., Mohinddin, T.M.G., Ponomarenko, L.A., Elias, D.C., Yang, R., Barbolina, I.I., Blake, P., Booth, T.J., Jiang, D., Giesbers, J., Hill, E.W. and Geim, A.K. “Electronic properties of graphene”, *Phys. Status Solidi B-Basic Solid State Phys.*, **244**(11), pp. 4106-4111 (2007).
 42. Balandin, A.A., Ghosh, S., Bao, W.Z., Calizo, I., Teweldebrhan, D., Miao, F. and Lau, C.N. “Superior thermal conductivity of single-layer graphene”, *Nano Lett.*, **8**(3), pp. 902-907 (2008).
 43. Zhu, Y., Murali, S., Cai, W., Li, X., Suk, J.W., Rotts, J.R. and Ruoff, R.S. “Synthesis and characterization of large-area graphene and graphite films on commercial Cu-Ni alloy foils”, *Adv. Mater.*, **22**(35), pp. 3906-3924 (2010).
 44. Jana, N.R. “Gram-scale synthesis of soluble, near-monodisperse gold nanorods and other anisotropic nanoparticles”, *Small*, **1**(8), pp. 875-882 (2005).
 45. Namazi, H. and Adeli, A. “Synthesis of barbell-like triblock copolymers, dendritic triazine -block-Poly(ethylene glycol)-block- dendritic triazine and investigation of their solution”, *Behaviors Polymer*, **46**(24), pp. 10788-10799 (2005).
 46. Namazi, H. and Adeli, M. “Solution proprieties of dendritic triazine/poly(ethylene glycol)/dendritic triazine block copolymers”, *J. Polym. Sci., Part A: Polym. Chem.*, **43**(1), pp. 28-41 (2005).
 47. Adeli, M., Zarnegar, Z. and Kabiri, R. “Dendritic macromolecules containing several types of functional groups”, *J. Appl. Polym. Sci.*, **115**(1), pp. 9-14 (2010).
 48. Hummers Jr, W.S. and Offeman, R.E. “Preparation of graphitic oxide”, *J. Am. Chem. Soc.*, **80**(6), pp. 1339-1339 (1958).
 49. Attal, S., Thiruvengadathan, R. and Regev, O. “Determination of the concentration of single-walled carbon nanotubes in aqueous dispersions using UV-visible absorption spectroscopy”, *Anal. Chem.*, **78**(23), pp. 8098-104 (2006).

50. Reed, B.W. and Sarikaya, M. “Electronic properties of carbon nanotubes by transmission electron energy-loss spectroscopy”, *Phys Rev B*, **64**(19), pp. 195404-1-195404-13 (2001).
51. Becerril, H.A., Mao, J., Liu, Z., Stoltenberg, R.M., Bao, Z. and Chen, Y. “Evaluation of solution-processed reduced graphene oxide films as transparent conductors”, *ACS Nano*, **2**(3), pp. 463-470 (2008).
52. Taflove, A. and Hagness, S.C. “The finite difference time-domain method, artech house publishers”, *Computational Electrodynamics*, p. 1006 (2005).
53. Johnson, P.B. and Christy, R.W. “Optical constants of the noble metals”, *Physical Review B*, **6**(12), pp. 4370-4379 (1972).

Biographies

Mohsen Adeli received his undergraduate degree from Lorestan University (Iran) in 1996. He obtained his MS and PhD degrees from Tabriz University in 1998 and 2005, respectively. He was promoted to the rank of associate professor in 2010. Mohsen Adeli was awarded the Razi Prize (2011) and prize for the most developed professor in the chemistry (2012) administered by the Ministry of Health and Medical Education of Iran and Iran Nanotechnology Initiative Council, respectively.

He is Professor of organic chemistry at Lorestan University now.

Fahimeh Madani received her BS (2008) in Pure Chemistry from Lorestan University (Iran). Next, she studied her MS (2012) in Organic Chemistry at the Lorestan University. She performed her MS research in the field of nano chemistry which included synthesis of novel drug delivery systems based on gold nanomaterials under the supervision of Prof. Mohsen Adeli.

Pezhman Sasanpour received his BS (Electronics), MS (Communication) and PhD (Nanoelectronics) from Amir-Kabir University of Technology, Khaje-Nasir University of Technology and Sharif University of Technology, respectively, in 2001, 2005 and 2010. After 2 years as a Postdoctoral Research Fellow at Sharif University of Technology, he joined Medical Physics and Biomedical Eng. Department of Shahid Beheshti Medical University in 2012, where he is Assistant Professor. He is also resident researcher at Institute for Research in Fundamental Sciences (IPM). His current research interests include biosensors, biophotonic, plasmonic, bioelectromagnetism and numerical simulation.